Results in Nonlinear Analysis 6 (2023) No. 1, 131–154
https://doi.org/10.31838/rna/2023.06.01.012
Available online at www.nonlinear-analysis.com

Results in Nonlinear Analysis
ISSN 2636-7556

Peer Reviewed Scientific Journal

Effect of the rotation and inclined magnetic field on peristaltic slip flow of a Bingham fluid with heat transfer in asymmetric channel and porous medium

Mohammed Obayes Kadhim[a,*], Liqaa Z. Hummady[b]

[a]*University of Al-Qadisiyah, College of Science, Department of Mathematics, Al-Qadisiyah, Iraq;* [b]*University of Baghdad, Department of Mathematics, Baghdad, Iraq*

Abstract

This essay aims to describe the peristaltic behavior of Bingham's fluid in an asymmetric channel and porous material. It is believed that the liquid will flow through a porous medium and will be sensitive to a strong, angled magnetic field. Convectional circumstances and varying thermal conductivity were used to study heat transfer qualities. The low Reynolds number and lengthy wavelength dependence lead to a significant simplification of the nonlinear equations. The key characteristics of velocity, temperature, pressure gradient, and trapping are discussed, with a particular emphasis on the slip coefficient and the tilted magnetic number. Graphical discussion of these parameters' impact. Additionally, the entrapment phenomenon is examined. With rising slip coefficient values and falling magnetic field strengths, permeability, and yield stress coefficients the trapped bolus grows in size.

Keywords: Peristaltic flow, rotation, inclined magnetic field, Bingham

1. Introduction

The peristaltic mechanism is well-studied in the realm of fluid research because it has several uses in both physiological and industrial settings. Through aprogressive wave of stretching and reducing

Email addresses: m.m.96moh@gmil.com (Mohammed Obayes Kadhim)*; liqqa.hummady@sc.uobaghdad.edu.iq (Liqaa Z. Hummady)*

Received March 20, 2023; Accepted April 11, 2023; Online May 17, 2023

motion along the fluid-carrying tube channel, peristalsis promotes fluid flow inside the corresponding system. In biological systems, peristalsis is responsible for a variety of processes, such as the movement of food particles in the esophagus, the movement of chyme in the gut, the movement of cilia, the vasomotion of small capillaries, etc. The well-known examples of peristaltic flow in an industrial process are the movement of poisonous liquids, sanitary transport, sedimentation, and the movement of caustic liquids. Peristaltic flow can be seen in biomedical engineering in blood pumping devices, heart-lung machines, roller pumps, finger pumps, etc. Srivastava and Srivastava [1] carried out one of the first investigations on the subject, using a power-law model to examine the peristalsis through both uniform and non-uniform channels. Improper peristalsis is the primary contributor to the sterility of the human uterus, the thrombus improvement of blood, and the neurotic passage of microscopic organisms [2]. Sreenadh and Narahari [3] Two-layer fluid models were investigated to understand the peristaltic behavior of a Newtonian fluid in contact with a Bingham fluid. To examine the flow behavior in the unyielded plug area. For the Poiseuille flow of Bingham fluid through a two-dimensional channel with barely perceptible width changes, Frigaard and Ryan [4] discovered an asymptotic solution. In numerous applications, such as the transfer flow of corrosive fluids and sanitary fluids without coming into contact with the mechanical parts, the effect of heat during peristaltic mechanisms is a major area of research, and blood pumps inside heart-lung machines. Consequently, it is vital to take heat transmission into account when researching peristalsis, especially in biological systems. To that goal, several investigations on peristalsis using non-Newtonian fluids and taking into account heat transfer have been made. In [5], it was investigated how heat transfer affected the peristaltic motion of an electrically conducting fluid through a porous media. A vertical asymmetric porous channel under the impact of heat transfer was the subject of an analysis by Srinivas and Gayathri [6]. Mekheimer and colleagues [7] investigated how heat transfer affected the peristaltic flow of heat transfer over a vertical porous asymmetric channel. Elahi and associates. Mekheimer [8] investigated how a generated magnetic field affected a magneto micropolar fluid's peristaltic flow. Pandey and Chaube [9] also investigated the effects of an external magnetic field on the peristaltic flow of a micropolar fluid through a porous medium. Assessing the effects of magnetic fields on physiological systems is essential limits on how much you can be exposed to certain technologies. Since erythrocytes, a significant component of blood, are known to have bio magnetic characteristics, magnetic fields have been shown to significantly affect the peristaltic movement of blood. Due to this, efforts have been made to provide an explanation for why fluid undergoes peristalsis when subjected to magnetic fields. Abdelsalam et al. [10] examined the effects of a magnetic field on the peristaltic mechanism of an electrically conducting hyperbolic tangent fluid when applied with ion and hall slip. The effects of heat transfer and slip circumstances on MHD peristaltic transport were investigated by Srinivas et al. [11]. Lakshminarayana et al. The impact of slip and wall features on the peristaltic transport of an MHD Bingham fluid with heat transfer were explored in [12]. Understanding the effects of magnetohydrodynamics and heat transfer on the Bingham fluid flows with peristaltic slip in porous channels with flexible walls, Satyanarayana et al. [13] created a model. Furthermore, sucharitha et al. [14, 15], Hayat et al. [16], Riaz et al. [17], Srinivas and Kothandapani [18], and others have explored the impact of wall characteristics. Studied by P. Lakshminarayana et al. In an inclined tapering porous tube with elastic walls, [19] discusses the consequences of Joule heating and slip-on peristaltic flow of a Bingham fluid. The permeability of the transport medium is an additional factor of comparable importance, particularly for biological systems. Kothandapani and Srinivas [20] investigated the peristaltic mechanism in a porous medium to determine how the elastic wall characteristics affected the peristalsis of an MHD fluid while taking heat transmission into account. With consideration for the porous medium, the peristalsis in a rigid asymmetric vertical tube [21] and the effects of wall features and heat transmission on peristalsis [22] were both clarified by Srinivas et al. There has been research on fluid models by Bingham [23], Rabinowitsch [24], and Jeffrey [25]. The current study's authors tried to describe peristalsis for a Bingham fluid along a conduit's length with a severe inclination while taking porous media into account. The investigation has taken into account the impacts of heat transfer with convective boundary conditions. The work by Divya et al. [26] makes

the assumption that the fluid is subject to a magnetic field with a substantial inclination and flows within a porous media while describing the peristaltic behavior of a fluid in the Bingham equation with variable viscosity. The resulting perturbed solution of the system is shown, and any relevant parameter changes have been taken into consideration. Throughout the course of our investigation, we learned that prior studies had not taken into account the fluctuating aperistaltically produced Bingham fluid's viscosity and thermal conductivity as it moves through a porous medium and is influenced by an angled magnetic field.

2. Formulation the Problem

The electrically conducting Bingham fluid is supposed to flow in a two-dimensional channel made of porous material in order to formulate the problem. The peristaltic wave train forces the fluid to flow, which is traveling with a constant speed of C. Additionally, it is assumed that the fluid motion is subject to a magnetic field, whose strength is indicated by the symbol B_0 in the transverse direction. For the channel and magnetic field, inclinations of γ and $\varnothing$ are taken into account, respectively. It is believed that the channel is symmetric around the axis. Additionally, because the Reynolds number is thought to be relatively tiny, we are able to ignore the induced magnetic field. The region of channel between the axes $y = 0$ and $y = y_p$ is referred to as the plug flow region. Where $|\tau_{xy}| \leq \tau_0$. For the region encapsulated by y_p and $\overline{h_1}, \overline{h_2}$, $|\tau_{xy}| > \tau_0$. The deformation in the channel walls caused by the peristaltic waves is modeled as in Figure 1.

$$\overline{h_1}(\bar{x}, \bar{t}) = E_1 - r_1 \sin\left[\frac{2\pi}{\lambda}(\bar{x} - c\bar{t})\right] \quad \text{upper wall,} \tag{1}$$

while at the lower wall is given by.

$$\overline{h_2}(\bar{x}, \bar{t}) = -E_2 - r_2 \sin\left[\frac{2\pi}{\lambda}(\bar{x} - c\bar{t}) + \varnothing\right] \quad \text{lower wall.} \tag{2}$$

where (r_1) and (r_2) indicate the wave's amplitudes, (E_1) and (E_2) denotes the channel's width, (λ) specifying the wavelength, The direction of the wave's propagation is represented by $(\bar{X})$, while the time

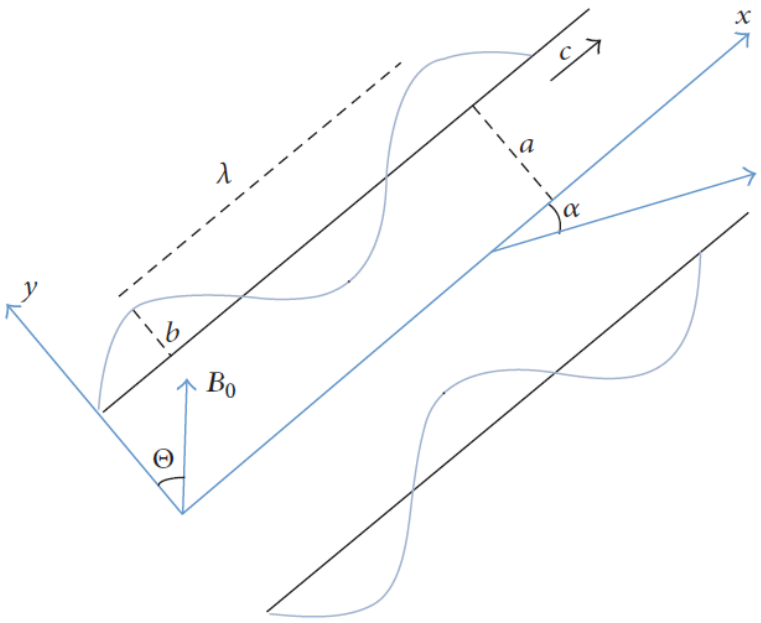

Figure 1: Geometry of the problem.

is indicated by $(\bar{t})$. The difference in phase $(\varnothing)$ varies across the range $(0 \le \varnothing \le \pi)$ in which $(\varnothing = 0)$ is equivalent to an out-of-phase, asymmetric channel and $(\varnothing = \pi)$ stands for the phase of the waves. Further (r_1), (r_2), (E_1), (E_2), and $(\varnothing)$ satisfy the condition:

$$r_1^2 + r_2^2 + 2r_1 r_2 \cos i(\varnothing) \le (E_1 + E_2)^2. \tag{3}$$

where a denotes the channel's half-width, b the amplitude, c the wave speed, and t the period. where V and v are the components of velocity in the transverse direction in the fixed and wave frames, respectively, and U, u is the axial velocity component in the laboratory and wave frames, respectively.

$$x = X - ct,\ y = Y,\ u = U - c,\ v = V \text{ and } p\ (x, y) = P\ (X,\ Y,\ t) \tag{4}$$

In the fixed and wave frames, the transverse velocity components are, respectively. These are the equations that control fluid flow in the wave frame.

$$\frac{\partial \bar{u}}{\partial \bar{x}} + \frac{\partial \bar{v}}{\partial \bar{y}} = 0 \tag{5}$$

The $\bar{x}$ –part of the moment equation is:

$$\begin{aligned} &\rho\left(\frac{\partial}{\partial \bar{t}} + \bar{u}\frac{\partial}{\partial \bar{x}} + \bar{v}\frac{\partial}{\partial \bar{y}}\right)\bar{u} - \rho\Omega\left(\Omega\bar{u} + 2\frac{\partial \bar{v}}{\partial \bar{t}}\right) \\ &= -\frac{\partial \bar{p}}{\partial \bar{x}} + \frac{\partial}{\partial \bar{x}}\bar{s}_{\bar{x}\bar{x}} + \frac{\partial}{\partial \bar{y}}\bar{s}_{\bar{x}\bar{y}} - \sigma B_0{}^2 \cos\beta^*(\bar{u}\ \cos\beta^* - \bar{v}\ \sin\beta^*) - \frac{\mu}{\bar{k}}\bar{u} \end{aligned} \tag{6}$$

The $\bar{y}$–part of the moment equation is:

$$\begin{aligned} &\rho\left(\frac{\partial}{\partial \bar{t}} + \bar{u}\frac{\partial}{\partial \bar{x}} + \bar{v}\frac{\partial}{\partial \bar{y}}\right)\bar{v} - \rho\Omega\left(\Omega\bar{v} + 2\frac{\partial \bar{u}}{\partial \bar{t}}\right) \\ &= -\frac{\partial \bar{p}}{\partial \bar{x}} + \frac{\partial}{\partial \bar{x}}\bar{s}_{\bar{x}\bar{y}} + \frac{\partial}{\partial \bar{y}}\bar{s}_{\bar{y}\bar{y}} - \sigma B_0{}^2 \cos\beta^*(\bar{u}\ \cos\beta^* - \bar{v}\ \sin\beta^*) - \frac{\mu}{\bar{k}}\bar{v} \end{aligned} \tag{7}$$

The energy equation:

$$\rho c_p\left(\frac{\partial}{\partial \bar{t}} + \bar{u}\frac{\partial}{\partial \bar{x}} + \bar{v}\frac{\partial}{\partial \bar{y}}\right)\bar{T} = k'\left(\frac{\partial^2}{\partial \bar{x}^2} + \frac{\partial^2}{\partial \bar{y}^2}\right)\bar{T} + \bar{s}_{\bar{x}\bar{x}}\left(\frac{\partial \bar{u}}{\partial \bar{x}}\right) + \bar{s}_{\bar{x}\bar{y}}\left(\frac{\partial \bar{v}}{\partial \bar{x}}\right) + \bar{s}_{\bar{x}\bar{y}}\left(\frac{\partial \bar{u}}{\partial \bar{y}}\right) + \bar{s}_{\bar{y}y}\left(\frac{\partial \bar{v}}{\partial \bar{y}}\right). \tag{8}$$

Where the $(\rho), (\bar{p}), (\mu), (\bar{k}), (B_0)$, (Ω) is constant density, pressure, dynamic viscosity, permeability parameter, constant magnetic field, rotation and $(\bar{u})$, $(\bar{v})$ are the velocities in X and Y paths in given frame.

3. Basic Equation

The fluid exhibits behavior consistent with the Bingham model, and the following information about its Cauchy stress tensor is given

$$\sigma = -PI + \bar{S} \tag{9}$$

$$\bar{S} = 2\mu\tau + 2\tau_0\hat{\tau} \tag{10}$$

In equation (5) τ_0 is the yield stress, and the tensor of rate of deformation τ and $\hat{\tau}$ is the tensor is described:

$$\hat{\tau} = \frac{\tau}{\sqrt{2\ \text{tras}\ \tau^2}} \tag{11}$$

$$\tau = \frac{1}{2}(\nabla \bar{V} + (\nabla \bar{V})^T) \tag{12}$$

Where (I) Identifier Tensor, $a(\partial \bar{X}, \partial \overline{Y}, 0)$ the gradient vector, ($\bar{P}$) the liquid's pressure and (μ) the dynamic viscosity".

$$\bar{s}_{\bar{x}\bar{x}} = 2\mu \bar{u}_{\bar{x}} + \frac{2\tau_0 \bar{u}_{\bar{x}}}{\sqrt{2\bar{u}_{\bar{x}}{}^2 + (\bar{v}_{\bar{x}} + \bar{u}_{\bar{y}})^2 + 2\bar{v}_{\bar{y}}{}^2}} \tag{13}$$

$$\bar{s}_{\bar{x}\bar{y}} = 2\mu \left(\frac{\bar{v}_{\bar{x}} + \bar{u}_{\bar{y}}}{2} \right) + \frac{2\tau_0 \left(\frac{\bar{v}_{\bar{x}} + \bar{u}_{\bar{y}}}{2} \right)}{\sqrt{2\bar{u}_{\bar{x}}{}^2 + (\bar{v}_{\bar{x}} + \bar{u}_{\bar{y}})^2 + 2\bar{v}_{\bar{y}}{}^2}} \tag{14}$$

$$\bar{s}_{\bar{y}\bar{y}} = 2\mu \bar{v}_{\bar{y}} + \frac{2\tau_0 \bar{v}_{\bar{y}}}{\sqrt{2\bar{u}_{\bar{x}}{}^2 + (\bar{v}_{\bar{x}} + \bar{u}_{\bar{y}})^2 + 2\bar{v}_{\bar{y}}{}^2}} \tag{15}$$

We use the following anon-dimensional quantities:

$$x = \frac{1}{\lambda}\bar{x},\ y = \frac{1}{E_1}\bar{y},\ u = \frac{1}{c}\bar{u},\ v = \frac{1}{\delta c}\bar{v},\ t = \frac{c}{\lambda}\bar{t},\ \delta = \frac{E_1}{\lambda},$$

$$\mathrm{Re} = \frac{\rho c E_1}{\mu},\ Da = \frac{\bar{k}}{E_1^2},\ \bar{T} = T - T_0,\ \theta = \frac{T - T_0}{T_1 - T_0},$$

$$Ec = \frac{c^2}{c_p\ (T_1 - T_0)},\ \mathrm{Pr} = \frac{\mu c_p}{k'},\ \eta = \frac{\Omega^2 E_1^2 \rho}{\mu},\ BR = \mathrm{Pr}\, Ec,\ \beta^* = \beta$$

$$s_{xx} = \frac{\lambda}{\mu c}\bar{s}_{\bar{x}\bar{x}},\ s_{xy} = \frac{E_1}{\mu c}\bar{s}_{\bar{x}\bar{y}},\ s_{yy} = \frac{E_1}{\mu c}\bar{s}_{\bar{y}\bar{y}},\ h_1 = \frac{1}{E_1}\overline{h_1},\ h_2 = \frac{1}{E_1}\overline{h_2},\ \boldsymbol{R}_n = \frac{\tau_0 E_1}{\mu c},\ p = \frac{E_1^2}{\lambda \mu c}\bar{p}. \tag{16}$$

Applying the aforementioned amounts to Eqs. (5)–(8), we obtain (after dropping the asterisks),

$$\frac{\partial u}{\partial x} + \frac{\partial v}{\partial y} = 0 \tag{17}$$

$$\begin{aligned} &\mathrm{Re}\,\delta\left(\frac{\partial u}{\partial t} + u\frac{\partial u}{\partial x} + v\frac{\partial u}{\partial y}\right) - \frac{\rho E_1^2}{\mu}\Omega^2 u - (2\Omega\delta^2\,\mathrm{Re})\left(\frac{\partial v}{\partial t}\right) \\ &= -\frac{\partial p}{\partial x} + \delta^2\frac{\partial}{\partial x}s_{xx} + \frac{\partial}{\partial y}s_{xy} - (Ha)^2\cos\beta^*(u\cos\beta^* - \delta v\sin\beta^*) - \frac{1}{Da}u \end{aligned} \tag{18}$$

$$\begin{aligned} &\mathrm{Re}\,\delta^3\left(\frac{\partial v}{\partial t} + u\frac{\partial v}{\partial x} + v\frac{\partial v}{\partial y}\right) - \frac{\rho E_1^2}{\mu}\delta^2\Omega^2 v - (2\Omega\delta^2\,\mathrm{Re})\left(\frac{\partial u}{\partial t}\right) \\ &= -\frac{\partial p}{\partial y} + \delta^2\frac{\partial}{\partial x}s_{xy} + \delta\frac{\partial}{\partial y}s_{yy} + Ha^2\sin\beta^*(\delta u\cos\beta^* - \delta^2 v\sin\beta^*) - \delta^2\frac{1}{Da}v \end{aligned} \tag{19}$$

$$\mathrm{Re}\,\delta\left(\frac{\partial}{\partial t} + u\frac{\partial}{\partial x} + v\frac{\partial}{\partial y}\right)\theta = \frac{1}{p_r}\left(\delta^2\frac{\partial^2}{\partial x^2} + \frac{\partial^2}{\partial y^2}\right)\theta + Ec\left[\delta^2 s_{xx}\left(\frac{\partial u}{\partial x}\right) + \delta^2 s_{xy}\left(\frac{\partial v}{\partial x}\right) + s_{xy}\left(\frac{\partial u}{\partial y}\right) + s_{yy}\left(\frac{\partial v}{\partial y}\right)\delta\right] \tag{20}$$

Then, in view of Eq. (16), Eq. (1), (2), and (13) to (15) take the form:

$$h_1(x,t) = 1 - a\sin(2\pi x) \tag{21}$$

$$h_2(x,t) = -E_2 - b\sin(2\pi x + \varnothing) \tag{22}$$

$$s_{xx} = 2\delta\frac{\partial u}{\partial x} + \frac{2\delta R_n\left(\frac{\partial u}{\partial x}\right)}{\sqrt{2\delta^2\left(\frac{\partial u}{\partial x}\right)^2 + \left(\delta^2\frac{\partial v}{\partial x} + \frac{\partial u}{\partial y}\right)^2 + 2\delta^2\left(\frac{\partial v}{\partial y}\right)^2}} \tag{23}$$

$$s_{xy} = \left(\delta^2\frac{\partial v}{\partial x} + \frac{\partial u}{\partial y}\right) + \frac{R_n\left(\delta^2\frac{\partial v}{\partial x} + \frac{\partial u}{\partial y}\right)}{\sqrt{2\delta^2\left(\frac{\partial u}{\partial x}\right)^2 + \left(\delta^2\frac{\partial v}{\partial x} + \frac{\partial u}{\partial y}\right)^2 + 2\delta^2\left(\frac{\partial v}{\partial y}\right)^2}} \tag{24}$$

$$s_{yy} = 2\delta\frac{\partial v}{\partial y} + \frac{2\delta R_n\left(\frac{\partial v}{\partial y}\right)}{\sqrt{2\delta^2\left(\frac{\partial u}{\partial x}\right)^2 + \left(\delta^2\frac{\partial v}{\partial x} + \frac{\partial u}{\partial y}\right)^2 + 2\delta^2\left(\frac{\partial v}{\partial y}\right)^2}} \tag{25}$$

The relations establish a connection between the velocity components and stream function (ψ):

$$u = \partial\psi/\partial y, v = -\partial\psi/\partial x. \tag{26}$$

Substituted Eqs. (26) in Eqs. (17), (18), (19), (20), (23), (24), (25) respectively,

$$\frac{\partial^2\psi}{\partial x\partial y} - \frac{\partial^2\psi}{\partial x\partial y} = 0 \tag{27}$$

$$\begin{aligned}&\mathrm{Re}\,\delta\left(-\frac{\partial^2\psi}{\partial t\partial y} + \frac{\partial^3\psi}{\partial x\partial y^2} - \frac{\partial^3\psi}{\partial x\partial y^2}\right) - \frac{\rho E_1^2}{\mu}\Omega^2\frac{\partial\psi}{\partial y} - (2\Omega\delta^2\,\mathrm{Re})\left(\frac{\partial^2\psi}{\partial t\partial x}\right)\\ &= -\frac{\partial p}{\partial x} + \delta^2\frac{\partial}{\partial x}s_{xx} + \delta\frac{\partial}{\partial y}s_{xy} + (Ha)^2\cos\beta^*\left(\frac{\partial\psi}{\partial y}\cos\beta^* + \delta^2\frac{\partial\psi}{\partial x}\sin\beta^*\right) + \frac{1}{Da}\frac{\partial\psi}{\partial y},\end{aligned} \tag{28}$$

$$\begin{aligned}&\mathrm{Re}\,\delta^3\left(-\frac{\partial^2\psi}{\partial t\partial x} + \frac{\partial^3\psi}{\partial x^2\partial y} - \frac{\partial^3\psi}{\partial x^2\partial y}\right) + \frac{\rho E_1^2}{\mu}\delta^2\Omega^2\frac{\partial\psi}{\partial x} - (2\Omega\delta^2\,\mathrm{Re})\left(\frac{\partial^2\psi}{\partial t\partial y}\right)\\ &= -\frac{\partial p}{\partial y} + \delta^2\frac{\partial}{\partial x}s_{xy} + \delta\frac{\partial}{\partial y}s_{yy} + (Ha)^2\sin\beta^*\left(\delta\frac{\partial\psi}{\partial y}\cos\boldsymbol{\beta}^* + \delta^2\frac{\partial\psi}{\partial x}\sin\beta^*\right) + \delta^2\frac{1}{Da}\frac{\partial\psi}{\partial x},\end{aligned} \tag{29}$$

$$\begin{aligned}&\mathrm{Re}\,\delta\left(\frac{\partial}{\partial t} + \frac{\partial^2\psi}{\partial x\partial y} - \frac{\partial^2\psi}{\partial x\partial y}\right)\theta = \frac{1}{p_r}\left(\delta^2\frac{\partial^2}{\partial x^2} + \frac{\partial^2}{\partial y^2}\right)\theta\\ &+\boldsymbol{Ec}\left[\delta^2 s_{xx}\left(\frac{\partial^2\psi}{\partial x\partial y}\right) - \delta^2 s_{xy}\frac{\partial^2\psi}{\partial x^2} + \delta^2 s_{xy}\left(\frac{\partial^2\psi}{\partial y^2}\right)^2 - \delta^2 s_{yy}\left(\frac{\partial^2\psi}{\partial x\partial y}\right)\right]\end{aligned} \tag{30}$$

$$s_{xx} = (2\delta)\frac{\partial^2\psi}{\partial x\partial y} + \frac{2\delta R_n\left(\frac{\partial^2\psi}{\partial x\partial y}\right)}{\sqrt{2\delta^2\left(\frac{\partial^2\psi}{\partial x\partial y}\right)^2 + \left(-\delta^2\frac{\partial^2\psi}{\partial x^2} + \frac{\partial^2\psi}{\partial y^2}\right)^2 + 2\delta^2\left(-\frac{\partial^2\psi}{\partial x\partial y}\right)^2}} \tag{31}$$

$$s_{xy} = \left(-\delta^2\frac{\partial^2\psi}{\partial x^2} + \frac{\partial^2\psi}{\partial y^2}\right) + \frac{R_n\left(-\delta^2\frac{\partial^2\psi}{\partial x^2} + \frac{\partial^2\psi}{\partial y^2}\right)}{\sqrt{\delta^2\left(\frac{\partial^2\psi}{\partial x\partial y}\right)^2 + \left(-\delta^2\frac{\partial^2\psi}{\partial x^2} + \frac{\partial^2\psi}{\partial y^2}\right)^2 + 2\delta^2\left(-\frac{\partial^2\psi}{\partial x\partial y}\right)^2}} \tag{32}$$

$$s_{yy} = -\delta\frac{\partial^2\psi}{\partial x\partial y} + \frac{2\delta R_n\left(\frac{\partial^2\psi}{\partial x\partial y}\right)}{\sqrt{\delta^2\left(\frac{\partial^2\psi}{\partial x\partial y}\right)^2 + \left(-\delta^2\frac{\partial^2\psi}{\partial x^2} + \frac{\partial^2\psi}{\partial y^2}\right)^2 + 2\delta^2\left(-\frac{\partial^2\psi}{\partial x\partial y}\right)^2}} \tag{33}$$

The wave frames dimensionless slip boundary conditions are

$$\begin{aligned} &\psi = \frac{F}{2} \text{ at } y = h_1 \ \psi = -\frac{F}{2} \text{ at } y = h_2, \\ &\frac{\partial\psi}{\partial y} + \beta_1\frac{\partial^2\psi}{\partial y^2} = -1 \text{ at } y = h_1, \frac{\partial\psi}{\partial y} - \beta_1\frac{\partial^2\psi}{\partial y^2} = -1 \text{ at } y = h_2, \\ &\frac{\partial\theta}{\partial y} = 0 \text{ at } y = 0, \frac{\partial\theta}{\partial y} + Bi\theta = 0 \text{ at } y = h_1, y = h_2 \end{aligned} \tag{34}$$

β_1 is the dimensionless slip parameter.

4. Solution of the Problem

It is impossible to provide a precise answer for each of the random parameters involved. We take perturbation strategy to get the answer. We go beyond treating the disorder.

$$\begin{aligned} \psi &= \psi_0 + R_n\psi_1 + O(R_n{}^2) \\ F &= F_0 + R_nF_1 + O(R_n{}^2), \\ p &= p_0 + R_np_1 + O(R_n{}^2). \end{aligned} \tag{35}$$

Substitute the terms (35) into Eqs. (27)–(33), and the equations for the boundary conditions (34) ($\delta \ll 1$), Due to the fact that higher order components it involves the power of (δ) is lower and negligible, we may construct by equating the coefficients of the following system of equivalent powers (Re):

From Eq. (32) and (28) we get:

$$\frac{dp}{dx} = \eta\psi_y + \psi_{yyy} + R_n\psi_y - B_n\psi_y \tag{36}$$

$$\eta = \frac{(\Omega^2 d^2\rho)}{\mu} \tag{37}$$

$$B_n = Ha^2 \cos^2 \beta^* + \frac{1}{Da} \tag{38}$$

From differential of y for Eq. (36)

$$0 = \psi_{yyyy} + R_n \psi_{yy} - B_n \psi_{yy} + \eta \psi_{yy} \tag{39}$$

From Eq. (29) we get:

$$-\frac{\partial p}{\partial y} = 0 \tag{40}$$

From Eq. (29) we get:

$$\theta_{yy} = -B_r s_{xy} \psi_{yy} \tag{41}$$

Zero Order System

When the order's terms are (R_n) are trivial in the system of zeroth order, we obtain:

$$\psi_{0yyyy} - B_n \psi_{0yy} + \eta \psi_{0yy} = 0 \tag{42}$$

Such that

$$\psi_0 = F_0/2,\ \partial\psi_0/\partial y = -1 \text{ at } y = h_1 \text{ and}$$

$$\psi_0 = -F_0/2,\ \partial\psi_0/\partial y = -1 \text{ at } y = h_2$$

$$\frac{\partial \psi_0}{\partial y} + \beta_1 \frac{\partial^2 \psi_0}{\partial y^2} = -1 \text{ at } y = h_1, \frac{\partial \psi_0}{\partial y} - \beta_1 \frac{\partial^2 \psi_0}{\partial y^2} = -1 \text{ at } y = h_2$$

$$\theta 0\ (h_1) = 0,\ \theta 0\ (h_2) = 0 \tag{43}$$

First order system

$$\psi_{1yyyy} + \psi_{0yy} - B_n \psi_{1yy} + \eta \psi_{1yy} = 0 \tag{44}$$

$$\psi_{1yyyy} - B_n \psi_{1yy} + \eta \psi_{1yy} = -\psi_{0yy} \tag{45}$$

$$\psi_1 = F_1/2,\ \partial\psi_0/\partial y = -1 \text{ at } y = h_1 \text{ and}$$

$$\psi_1 = -F_1/2,\ \partial\psi_0/\partial y = -1 \text{ at } y = h_2$$

$$\frac{\partial \psi_1}{\partial y} + \beta_1 \frac{\partial^2 \psi_1}{\partial y^2} = -1 \text{ at } y = h_1 \frac{\partial \psi_1}{\partial y} - \beta_1 \frac{\partial^2 \psi_1}{\partial y^2} = -1 \text{ at } y = h_2,$$

$$\theta 1\ (h_1) = 0,\ \theta 1\ (h_2) = 0 \tag{46}$$

And by resolving the related zeroth and first order systems, you may obtain the final equation for the stream function:

$$\psi = \psi_0 + R_n \psi_1 \tag{47}$$

Where the functions (ψ_0, ψ_1) hefty expressions Consequently, they will be mentioned in Appendix.

$$\frac{\partial p}{\partial x} = \psi_{0yyy} + R_n\psi_{1yyy} + R_n\psi_{0yy} + {R_n}^2\psi_{0yy} - B_n\psi_{0y} + \eta\psi_{0y} - B_nR_n\psi_{1y} + \eta R_n\psi_{1y} \tag{48}$$

The definition of pressure increases per wave length (Δp) is

$$\Delta p = \int_0^1 \frac{dp}{dx}\, dx. \tag{49}$$

5. Results and Discussion

To investigate the impact of physical factors like Effect of, Darcy number (Da), Hartman number (Ha), Reynolds number (Re), inclination of magnetic field (β^*), Rotation (Ω), Porous medium parameter (k), Material fluid parameters (Rn), Density (ρ), Viscosity (μ), pressure rise (Δp), slip coefficient (β_1), the plotted axial velocity (u), phase difference ($\varnothing$) and stream function (ψ) in Figures 2–18 are exemplified by software "MATHEMATICA".

*5.1 Velocity Distribution (**u**)*

Figures 2–9 demonstrate how the axial velocity (u) value can vary with respect to y for various rotational values (Ω), Darcy number (Da), Viscosity (μ), material fluid parameter (Rn), inclination of magnetic field (β^*), slip coefficient (β_1), Hartman number (Ha), and amplitude ratio ($\varnothing$). These figures show that the maximum velocity is consistently found close to the channel's center and that All instances of the velocity profiles are parabolic. Figures 3, 4, and 7 show that the axial velocity decreases as (Ha), (Rn), and (β_1) increase. Figures 2, 5, and 8 show that raising the (Da), (Ω), and (β^*) raises axial velocity. Figures 6 and 9 The effect of ($\varnothing$) and (μ) when the speed increases, it starts decreasing at the left channel wall, then it merges with the other one in center, and then decreasing too at the right channel wall.

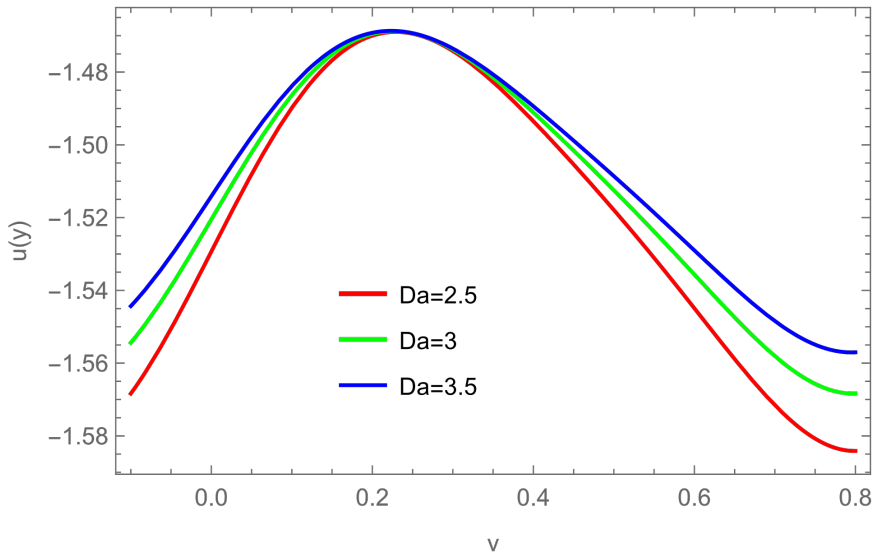

Figure 2: Variation of velocity for different values of Da when Ha = 0.4, Ω = 0.5, β* = 0.3, Rn = 0.5, μ = 1, β_1 = 0.2, ρ = 1, Ø = 1.5, a = 0.1, b = 0.3, E_1 = 0.5, E = 0.1.

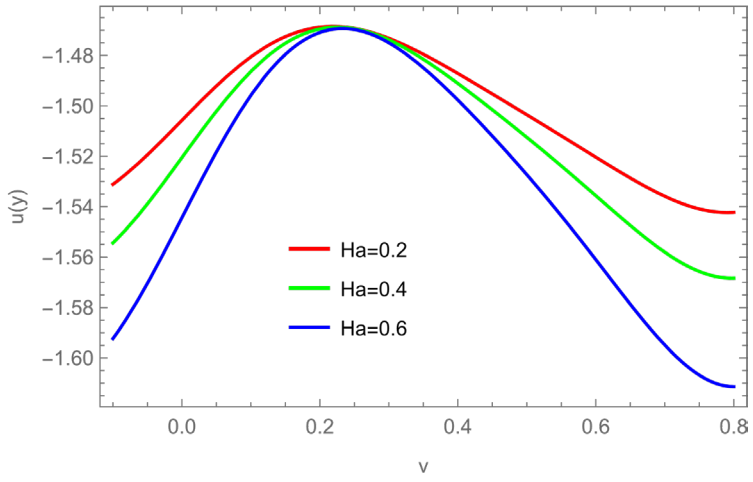

Figure 3: Variation of velocity for different values of Ha when Da = 3, Ω = 0.5, β^* = 0.3, Rn = 0.5, $\mu = 1$, $\beta_1 = 0.2$, $\rho = 1$, Ø = 1.5, $a = 0.1$, $b = 0.3$, $E_1 = 0.5$, $E = 0.1$.

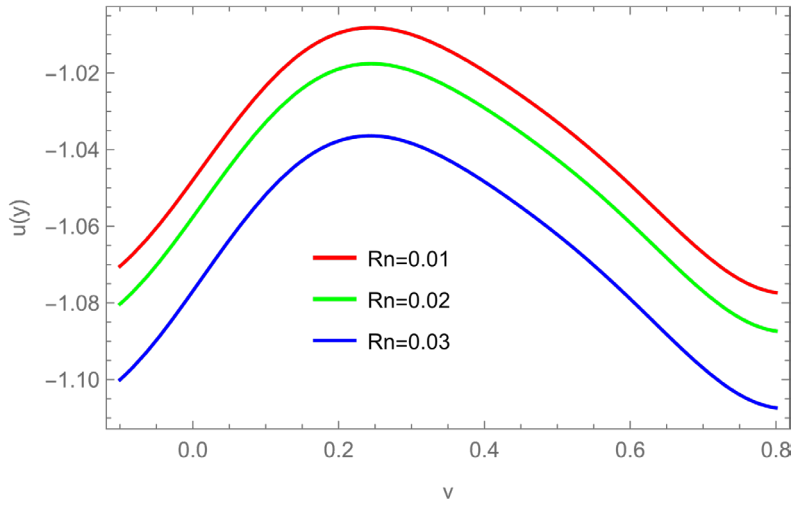

Figure 4: Variation of velocity for different values of Rn when Da = 3, Ω = 0.5, β^* = 0.3, Ha = 0.4, $\mu = 1$, $\beta_1 = 0.2$, $\rho = 1$, Ø = 1.5, $a = 0.1$, $b = 0.3$, $E_1 = 0.5$, $E = 0.1$.

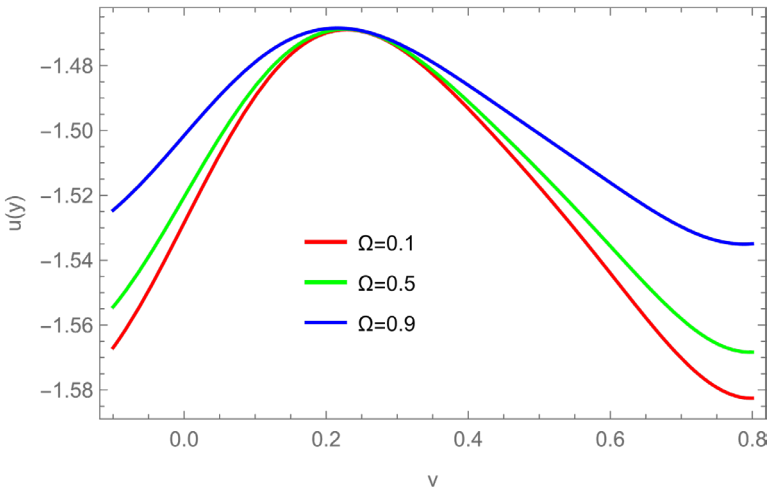

Figure 5: Variation of velocity for different values of Ω when Da = 3, Ha = 0.4, β^* = 0.3, Rn = 0.5, $\mu = 1$, $\beta_1 = 0.2$, $\rho = 1$, Ø = 1.5, $a = 0.1$, $b = 0.3$, $E_1 = 0.5$, $E = 0.1$.

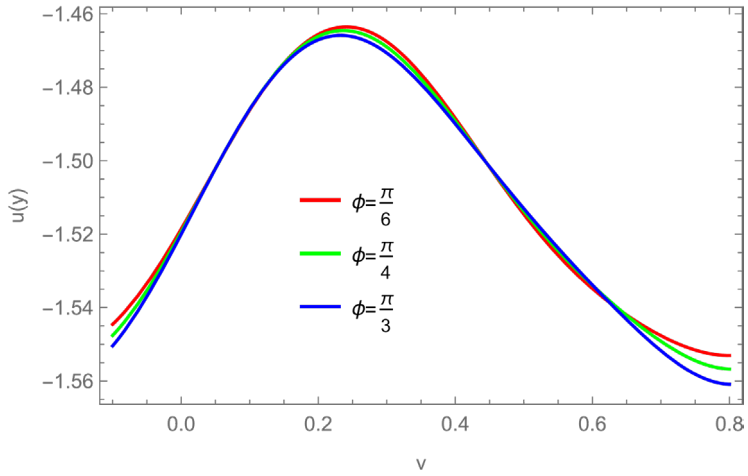

Figure 6: Variation of velocity for different values of Ø when Da = 3, Ha = 0.4, β^* = 0.3, Rn = 0.5, μ = 1, β_1 = 0.2, ρ = 1, Ω = 0.5, a = 0.1, b = 0.3, E_1 = 0.5, E = 0.1.

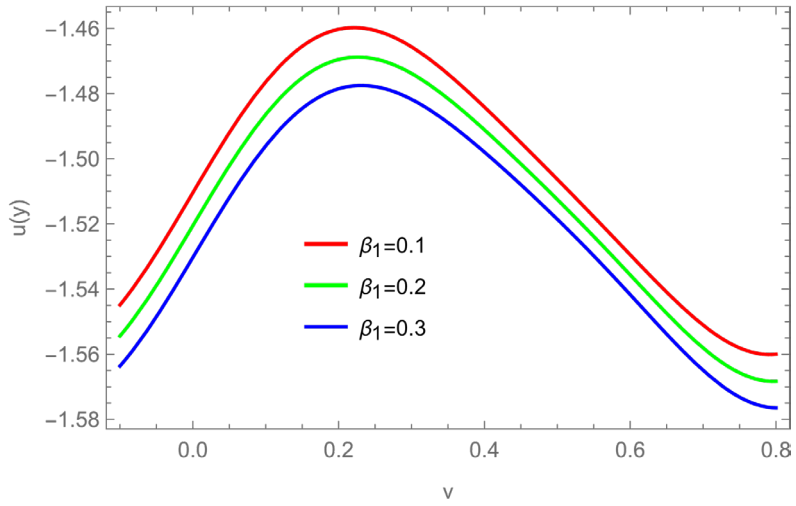

Figure 7: Variation of velocity for different values of β_1 when Da = 3, Ha = 0.4, β^* = 0.3, Rn = 0.5, μ = 1, Ω = 0.5, ρ = 1, Ø = 1.5, a = 0.1, b = 0.3, E_1 = 0.5, E = 0.1.

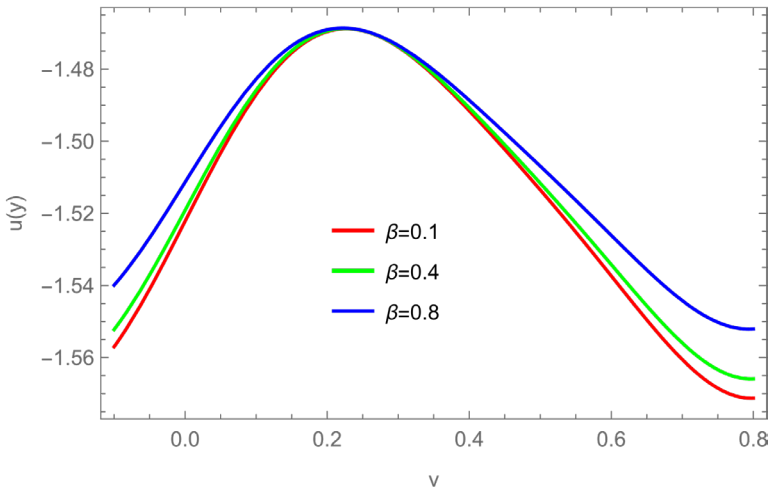

Figure 8: Variation of velocity for different values of β^* when Da = 3, Ha = 0.4, Ω = 0.5, Rn = 0.5, μ = 1, β_1 = 0.2, ρ = 1, Ø = 1.5, a = 0.1, b = 0.3, E_1 = 0.5, E = 0.1.

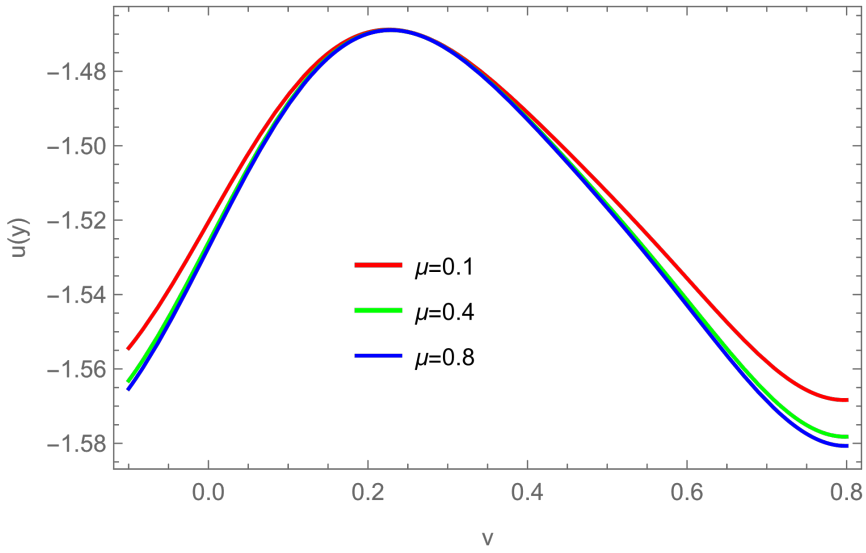

Figure 9: Variation of velocity for different values of μ when Da = 3, Ha = 0.4, β^* = 0.3, Rn = 0.5, $\Omega = 0.5$, $\beta_1 = 0.2$, $\rho = 1$, $\emptyset = 1.5$, $a = 0.1$, $b = 0.3$, $E_1 = 0.5$, $E = 0.1$.

5.2 Pressure Gradient

Graphical representation of the impact of relevant parameters on the pressure gradient (dp/dx) is possible Figures 10–17. The increasing values of the Darcy number (Da), the material fluid (Rn), the rotation (Ω), and the Density (ρ) led to a decrease in the pressure gradient. In Figures 10 and 15, we notice that the pressure gradient increases with increasing (Ha) and (β_1). Figure 16 shown is how ($\emptyset$) affects the axial pressure gradient (dp/dx). The increase in ($\emptyset$) is seen to cause a rise in (dp/dx) at the channel's left wall while a decline in (dp/dx) is seen on the right side. In Figure 17 there is no change in pressure when (μ).

5.3 Pressure Rise (Δp)

Figures 18–23 display the various pressure increases in the wave outline's capability of volumetric stream rate for various Darcy number (Da), Rotation (Ω), material fluid parameter (Rn), Density (ρ), Hartman number (Ha) and slip coefficient (β_1). The relationship between a dimensionless mean flow rate (Q1) and a non-dimensional average pressure rises per wavelength will be illustrated in this paragraph along with variations in the relevant parameters in (Δp). Figure 20 and 22 shows the effect of increasing the parameter (Ω) and (β_1) on (ΔP) reveals that pressure rice per wave length ΔP increase in magnitude in all regions. Figure 19 demonstrates that pressure increase (Δp) diminishes as (Da) In zone of increased pumping and the compounding region ($\Delta p < 0$), it is seen that pumping rises. According to Figure 18, the pumping rate increases in aretrograde region where ($\Delta p > 0$, Q1 > 0) and lowers in acop umping zone where ($\Delta p < 0$, Q1 < 0), according to the graph. As the magnetic field (Ha) expands, the pressure rises ($\Delta p > 0$). Figure 21 shows the pressure rice per wave length ΔP decreases in magnitude for fixed values of the (Rn). In Figure 17 there is no change in pressure when (ρ).

5.4 Temperature Distribution

Many variables are influenced by the temperature field, included Prandtl number (Pr), rotation (Ω), Eckert number (Ec), density (ρ), Hartman number (Ha), viscosity (μ), Darcy number (Da), phase difference ($\emptyset$), in Figures 24–31. The temperature field is seen in Figures 24, 27, and 28 to be growing at the channel's boundary while remaining unchanged in the channel's core region with increasing (Ha), (β), and (BR) values. In Figures 25 and 26, it is depicted that the temperature field in the channel's

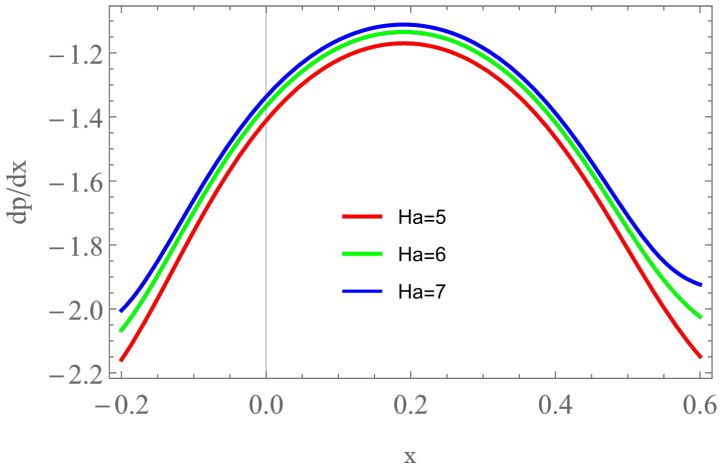

Figure 10: Variation of pressure gradient for different values of Ha when Da = 2, Ω = 0.5, β^* = 0.5, Rn = 0.3, μ = 0.6, β_1 = 3, ρ = 0.4, Ø = 0.4, a = 0.1, b = 0.3, E_1 = 0.5, E = 0.1.

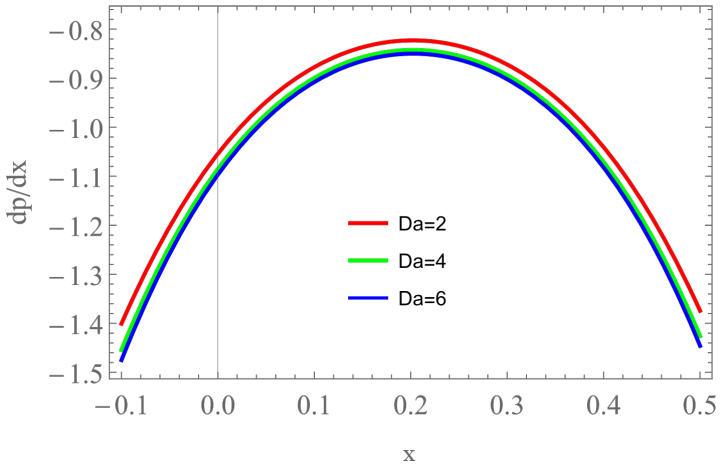

Figure 11: Variation of pressure gradient for different values of Da when Ha = 2, Ω = 0.5, β^* = 0.5, Rn = 0.3, μ = 0.6, β_1 = 3, ρ = 0.4, Ø = 0.4, a = 0.1, b = 0.3, E_1 = 0.5, E = 0.1.

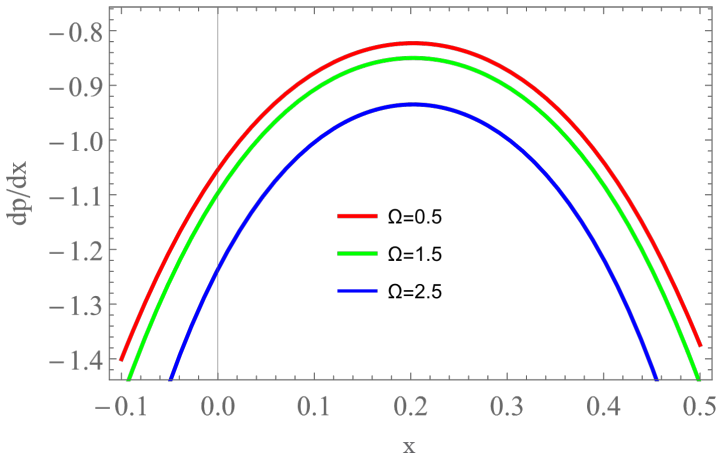

Figure 12: Variation of pressure gradient for different values of Ω when Ha = 2, Da = 2, β^* = 0.5, Rn = 0.3, μ = 0.6, β_1 = 3, ρ = 0.4, Ø = 0.4, a = 0.1, b = 0.3, E_1 = 0.5, E = 0.1.

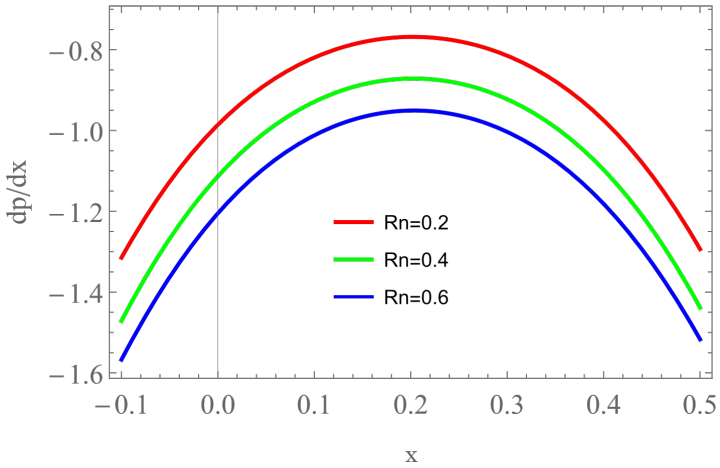

Figure 13: Variation of pressure gradient for different values of Rn when Ha = 2, Ω = 0.5, β^* = 0.5, Da = 2, μ = 0.6, β_1 = 3, ρ = 0.4, Ø = 0.4, a = 0.1, b = 0.3, E_1 = 0.5, E = 0.1.

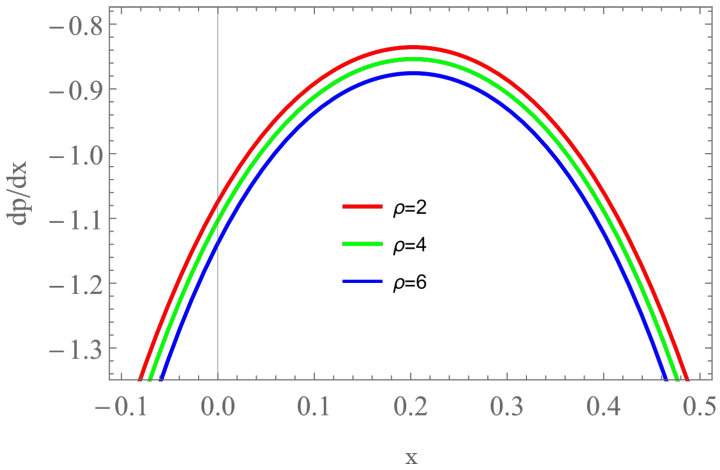

Figure 14: Variation of pressure gradient for different values of ρ when Ha = 2, Ω = 0.5, β^* = 0.5, Da = 2, μ = 0.6, β_1 = 3, Da = 2, Ø = 0.4, a = 0.1, b = 0.3, E_1 = 0.5, E = 0.1.

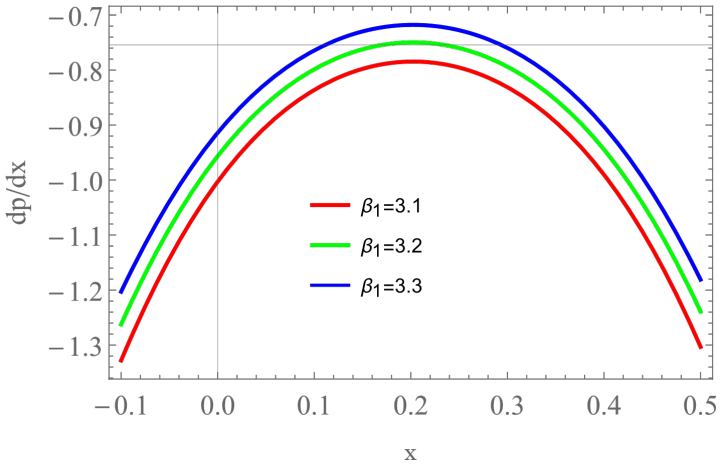

Figure 15: Variation of pressure gradient for different values of β_1 when Ha = 2, Ω = 0.5, β^* = 0.5, Da = 2, μ = 0.6, ρ = 0.4, Ø = 0.4, a = 0.1, b = 0.3, E_1 = 0.5, E = 0.1.

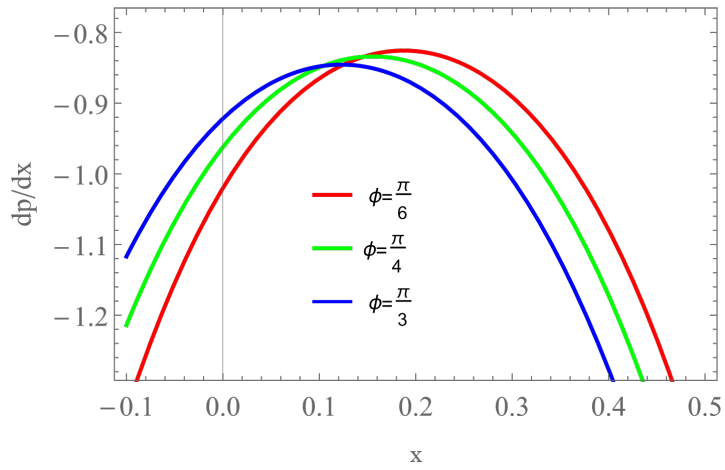

Figure 16: Variation of pressure gradient for different values of Ø when Ha = 2, Ω = 0.5, β^* = 0.5, Rn = 0.3, μ = 0.6, β_1 = 3, ρ = 0.4, Da = 2, a = 0.1, b = 0.3, E_1 = 0.5, E = 0.1.

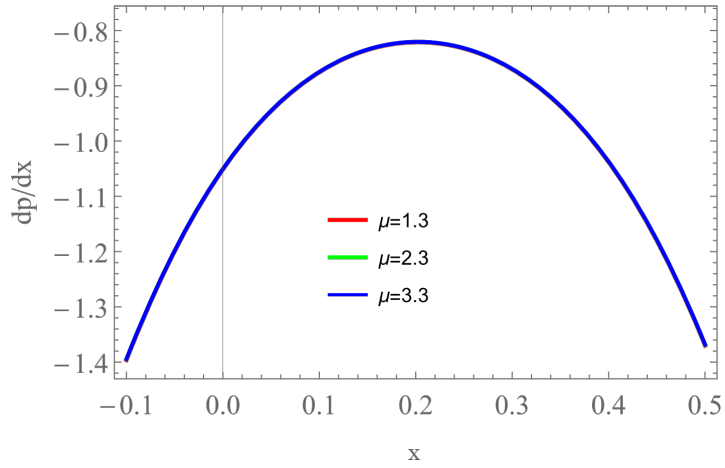

Figure 17: Variation of pressure gradient for different values of μ when Ha = 2, Ω = 0.5, β^* = 0.5, Rn = 0.3, Da = 2, β_1 = 3, ρ = 0.4, Ø = 0.4, a = 0.1, b = 0.3, E_1 = 0.5, E = 0.1.

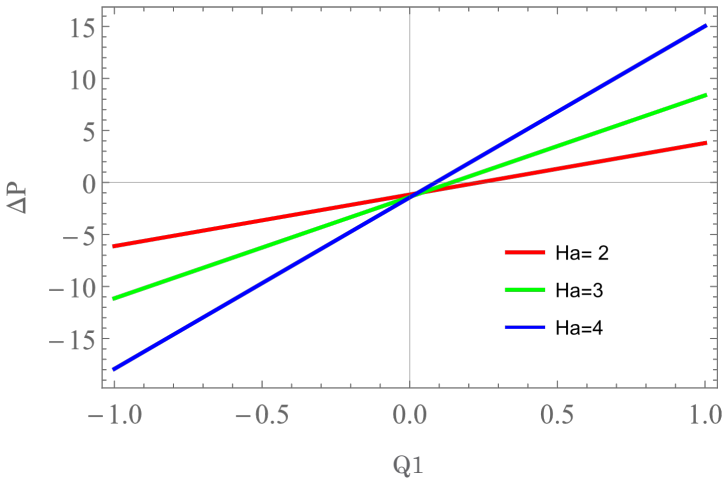

Figure 18: Variation of pressure rise ΔP with Q1 for different values of Ha when Da = 0.9, Ω = 0.7, β^* = 0.2, Rn = 0.3, μ = 0.6, β_1 = 3, ρ = 0.4, Ø = 0.4, a = 0.1, b = 0.3, E_1 = 0.5, E = 0.1.

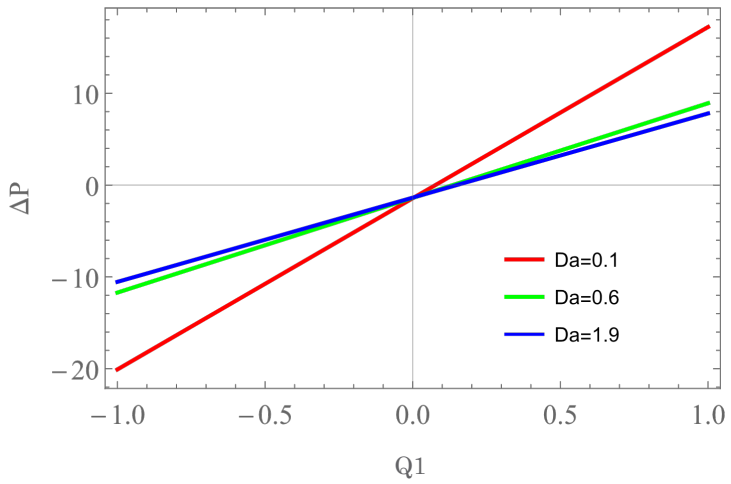

Figure 19: Variation of pressure rise ΔP with Q1 for different values of Da when Ha = 3, Ω = 0.7, β^* = 0.2, Rn = 0.3, μ = 0.6, β_1 = 3, ρ = 0.4, Ø = 0.4, a = 0.1, b = 0.3, E_1 = 0.5, E = 0.1.

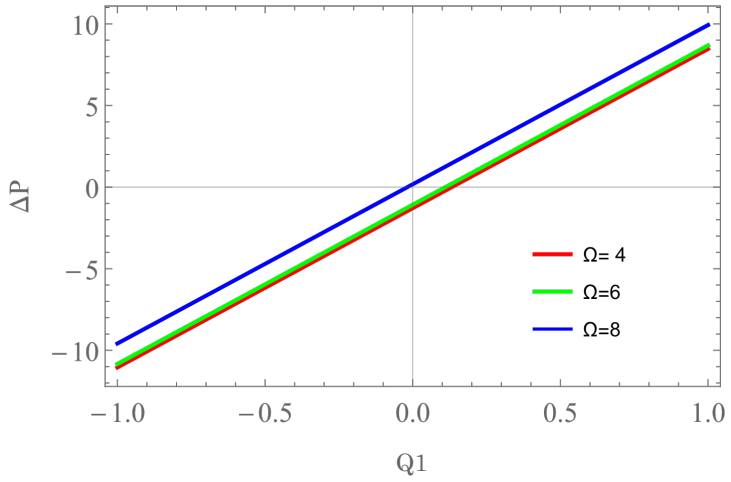

Figure 20: Variation of pressure rise ΔP with Q1 for different values of Ω when Da = 0.9, Ha = 3, β^* = 0.2, Rn = 0.3, μ = 0.6, β_1 = 3, ρ = 0.4, Ø = 0.4, a = 0.1, b = 0.3, E_1 = 0.5, E = 0.1.

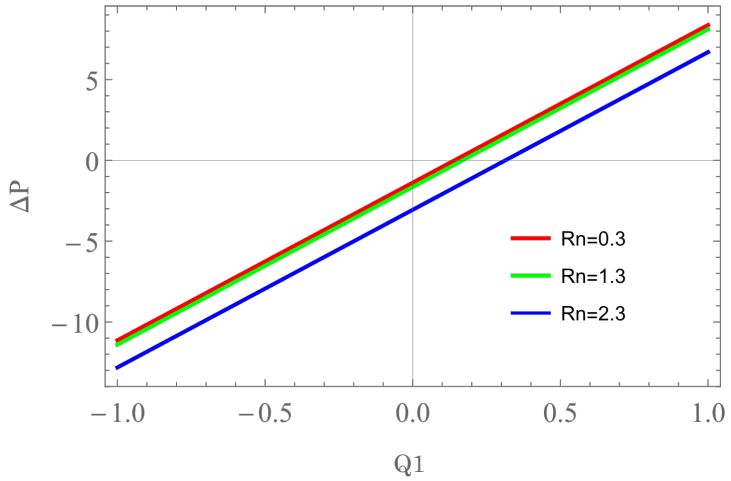

Figure 21: Variation of pressure rise ΔP with Q1 for different values of Rn when Da = 0.9, Ω = 0.7, β^* = 0.2, Ha = 3, μ = 0.6, β_1 = 3, ρ = 0.4, Ø = 0.4, a = 0.1, b = 0.3, E_1 = 0.5, E = 0.1.

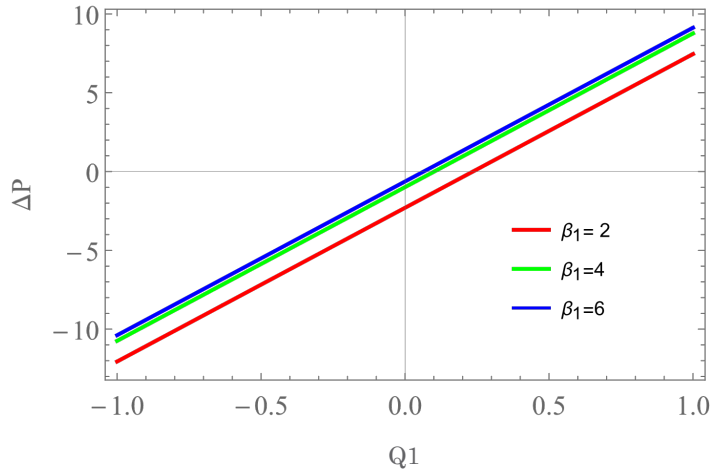

Figure 22: Variation of pressure rise ΔP with Q1 for different values of β_1 when Da = 0.9, Ω = 0.7, β^* = 0.2, Rn = 0.3, μ = 0.6, Ha = 3, ρ = 0.4, Ø = 0.4, a = 0.1, b = 0.3, E_1 = 0.5, E = 0.1.

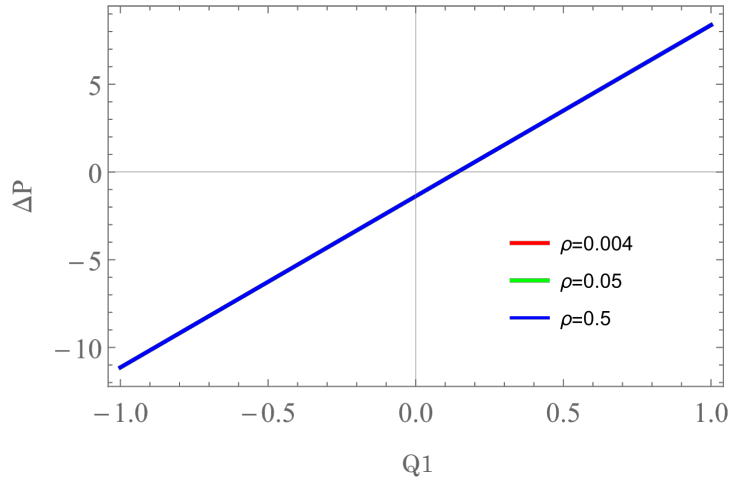

Figure 23: Variation of pressure rise ΔP with Q1 for different values of ρ when Da = 0.9, Ω = 0.7, β^* = 0.2, Rn = 0.3, μ = 0.6, β_1 = 3, Ha = 0.4, Ø = 0.4, a = 0.1, b = 0.3, E_1 = 0.5, E = 0.1.

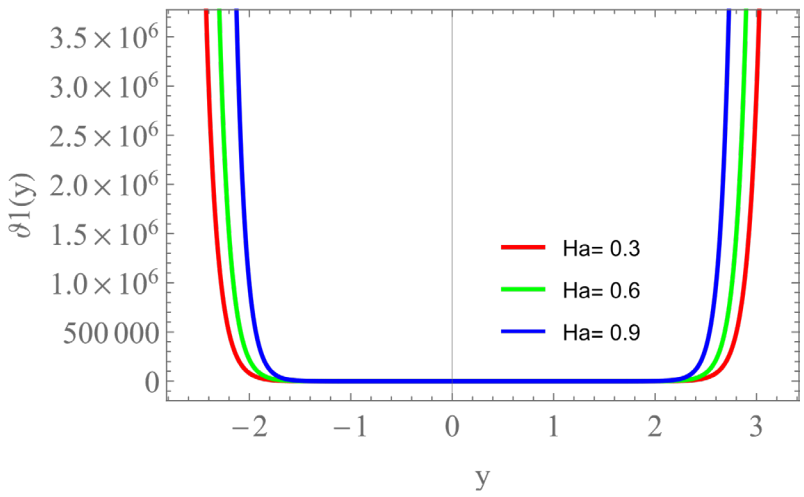

Figure 24: The variation of temperature θ with y for different values of Ha when Da = 0.6, β^* = 0.3, BR = 2, μ = 1, ρ = 1, Ω = 0.5, Ø = 1.5, a = 0.1, b = 0.3, E_1 = 0.5, E = 0.1.

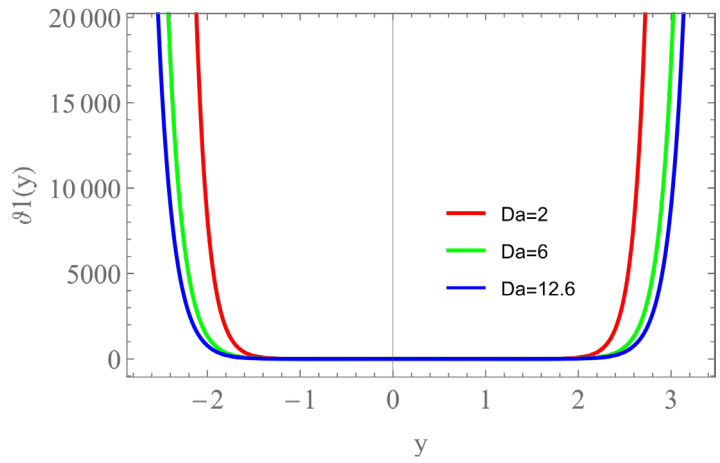

Figure 25: The variation of temperature θ with y for different values of Da when Ha = 0.9, β^* = 0.3, BR = 2, μ = 1, ρ = 1, Ω = 0.5, $\O$ = 1.5, a = 0.1, b = 0.3, E_1 = 0.5, E = 0.1.

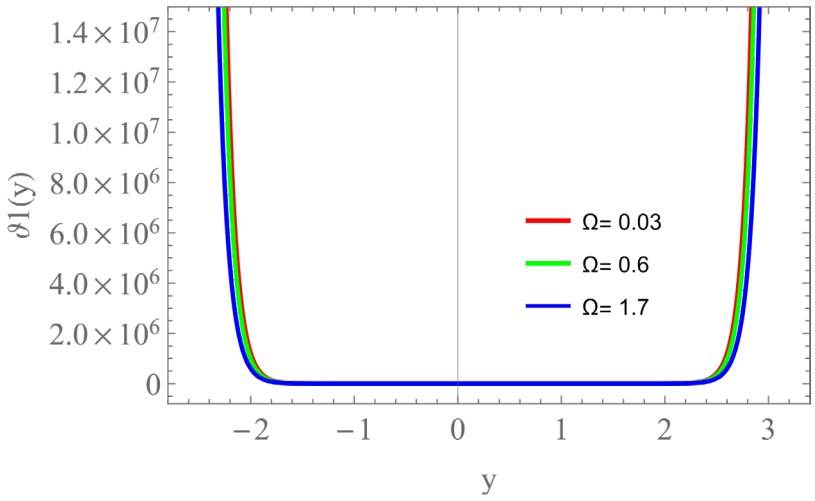

Figure 26: The variation of temperature θ with y for different values of Ω when Da = 0.6, β^* = 0.3, BR = 2, μ = 1, ρ = 1, Ha = 0.9, $\O$ = 1.5, a = 0.1, b = 0.3, E_1 = 0.5, E = 0.1.

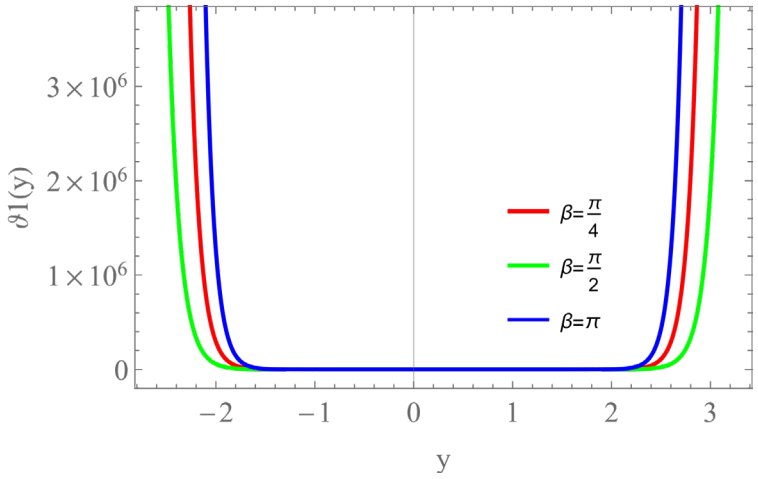

Figure 27: The variation of temperature θ with y for different values of β^* when Da = 0.6, Ha = 0.9, BR = 2, μ = 1, ρ = 1, Ω = 0.5, $\O$ = 1.5, a = 0.1, b = 0.3, E_1 = 0.5, E = 0.1.

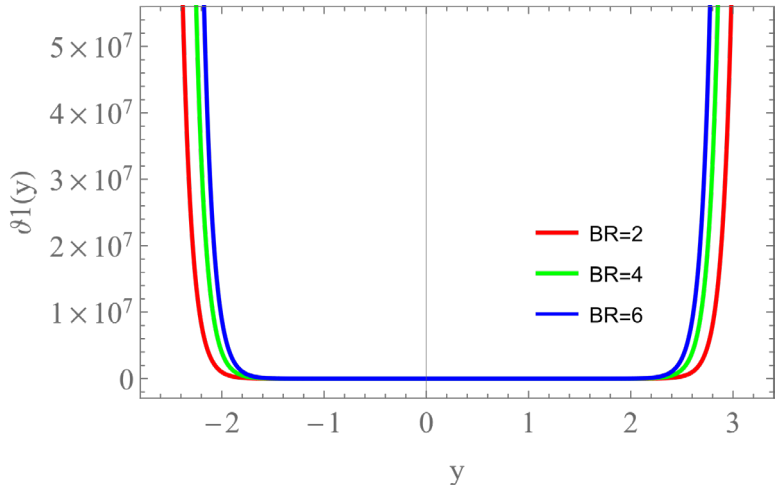

Figure 28: The variation of temperature θ with y for different values of BR when Da = 0.6, β^* = 0.3, Ha = 0.9, μ = 1, ρ = 1, Ω = 0.5, Ø = 1.5, a = 0.1, b = 0.3, E_1 = 0.5, E = 0.1.

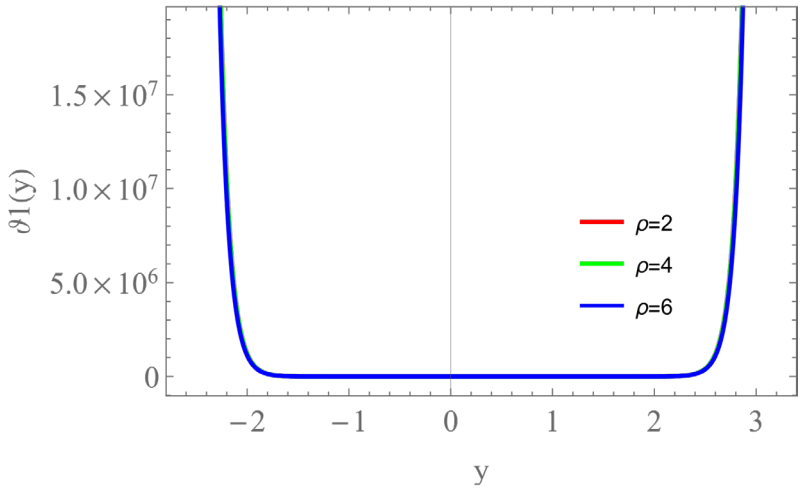

Figure 29: The variation of temperature θ with y for different values of ρ when Da = 0.6, β^* = 0.3, BR = 2, μ = 1, Ha = 0.9, Ω = 0.5, Ø = 1.5, a = 0.1, b = 0.3, E_1 = 0.5, E = 0.1.

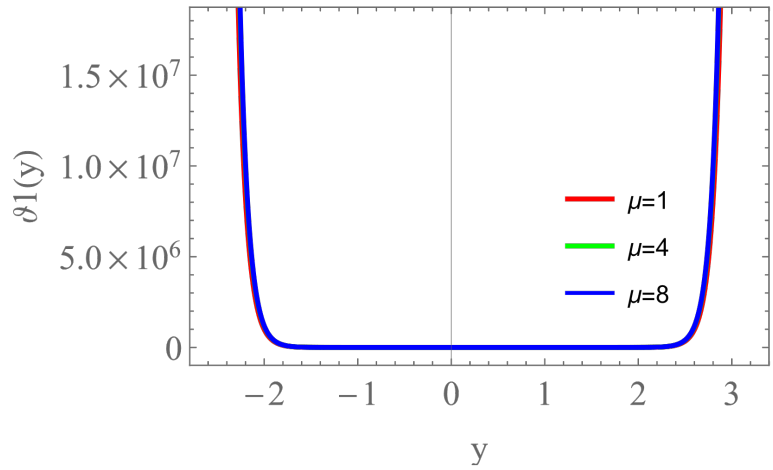

Figure 30: The variation of temperature θ with y for different values of μ when Da = 0.6, β^* = 0.3, BR = 2, Ha = 0.9, ρ = 1, Ω = 0.5, Ø = 1.5, a = 0.1, b = 0.3, E_1 = 0.5, E = 0.1.

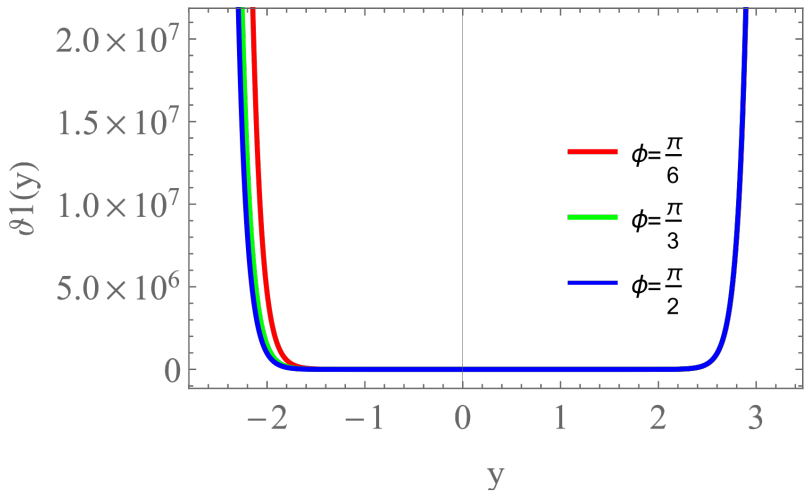

Figure 31: The variation of temperature θ with y for different values of Ø when Da = 0.6, β^* = 0.3, BR = 2, μ = 1, ρ = 1, Ω = 0.5, Ø = 1.5, Ha = 0.9, a = 0.1, b = 0.3, E_1 = 0.5, E = 0.1.

middle is increasing (Da), while the temperature field near the wall's boundary is decreasing. In Figure 31, the temperature field is depicted as growing (∅) with no change in the channel's middle on the right and left, and dropping (∅) in close proximity to the boundary on the left of the channel wall. From Figures 29 and 30 noted that the temperature field do not change at increasing in (ρ), (μ).

$$*\text{BR} = Pr\ Ec.$$

5.5 Trapping Phenomena

An interesting component happens in peristaltic flows closed movement strains lure bolus, or the extent of fluid called bolus, in the channel tube close to the partitions, and this trapping bolus advances along the path of the wave. In Figures 32–37 plots of the stream lines are shown at different values. of (Ω), (Da), (Rn), (Ha), (ρ) and (β_1). Figures 32, 34 and 37 it shows a shrinking of the trapped bolus when the (Ω), (Ha) and (ρ) is increased. Figures 33 and 35 the exhibits that the trapping exists in the focus of the channel, an increase in (Da) and (Rn) increases the size of bolus, Figure 36 also illustrates the influence of the slip parameter (β_1), with an increase in (β_1) resulting in a larger bolus.

6. Conclusions

The peristaltic motion of Bingham plastic fluid in an asymmetric channel with a porous material was examined in this study to determine the impact of magnetism and rotation on it. By choosing peristaltic waves with various ranges, phases, low Reynolds numbers, and wavelengths, the asymmetric duct is created. The expression for the axial velocity, magnetic force, flow function, and current density were also obtained using an application of the perturbation method. Graphs are used to illustrate the findings as follows:

1. Velocity is a decreasing function of the slip parameter β_1 whereas it is a increasing function of the Darcy number Da, rotation Ω and β.
2. Pressure gradient increases by increasing of the slip parameter β_1 and Hartman number Ha in the channel, whereas it is a decreasing function of the Darcy number Da, rotation Ω, density ρ and Rn.
3. The pressure rise enhances above the critical value of flow rate with higher values of Darcy number.
4. A rise in the fluid temperature and a decrease in heat transfer coefficient are caused by an increase in the variable thermal conductivity.
5. For higher values of Ω, Ha and ρ, the size of the trapped bolus decreases while it increases with increasing Da and Rn.

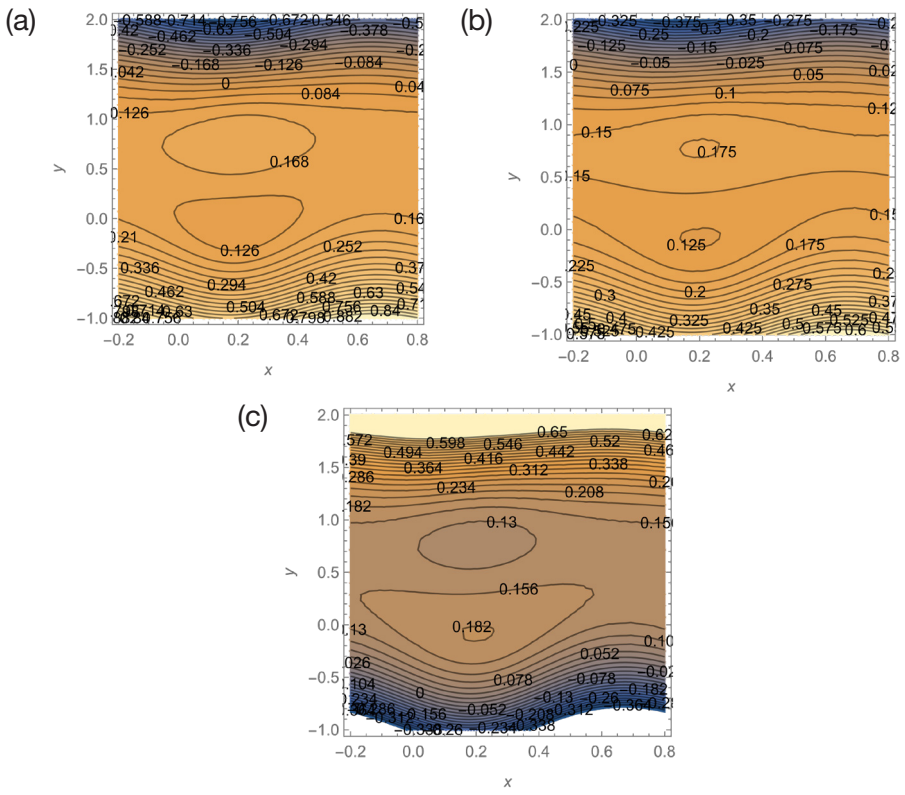

Figure 32: Stream function in the wave frame of (Ha) such that in (a) Ha = 0.1, (b) Ha = 0.4, (c) Ha = 0.8, in Ω = 2, Da = 6, $\mu = 0.6$, $\rho = 0.4$, Ø = 0.4, $a = 0.1$, $b = 0.3$, $d = 0.5$, $E_1 = 0.5$, $E = 0.1$, $\beta^* = 0.1$, Rn = 0.3, $\beta_1 = 0.2$.

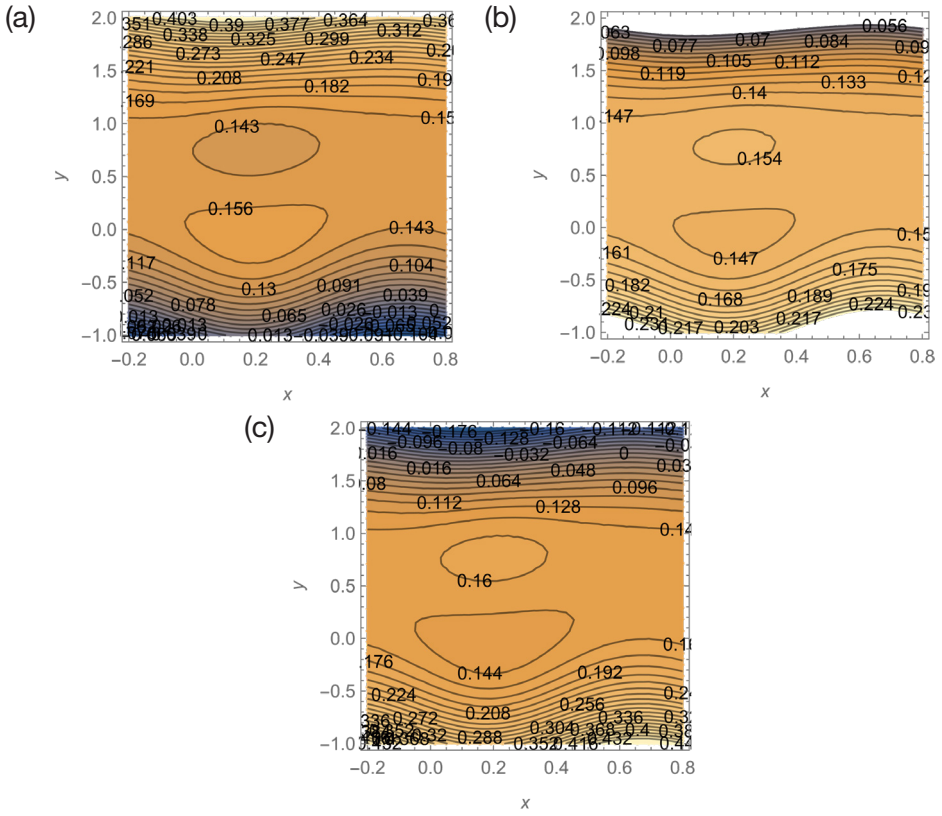

Figure 33: Stream function in the wave frame of (Da) such that in (a) Da = 2.2, (b) Da = 3.2, (c) Da = 4.2, in Ω = 2, Ha = 0.4, $\mu = 0.6$, $\rho = 0.4$, Ø = 0.4, a = 0.1, b = 0.3, $E_1 = 0.5$, $E = 0.1$, $\beta^* = 0.1$, Rn = 0.3, $\beta_1 = 0.2$.

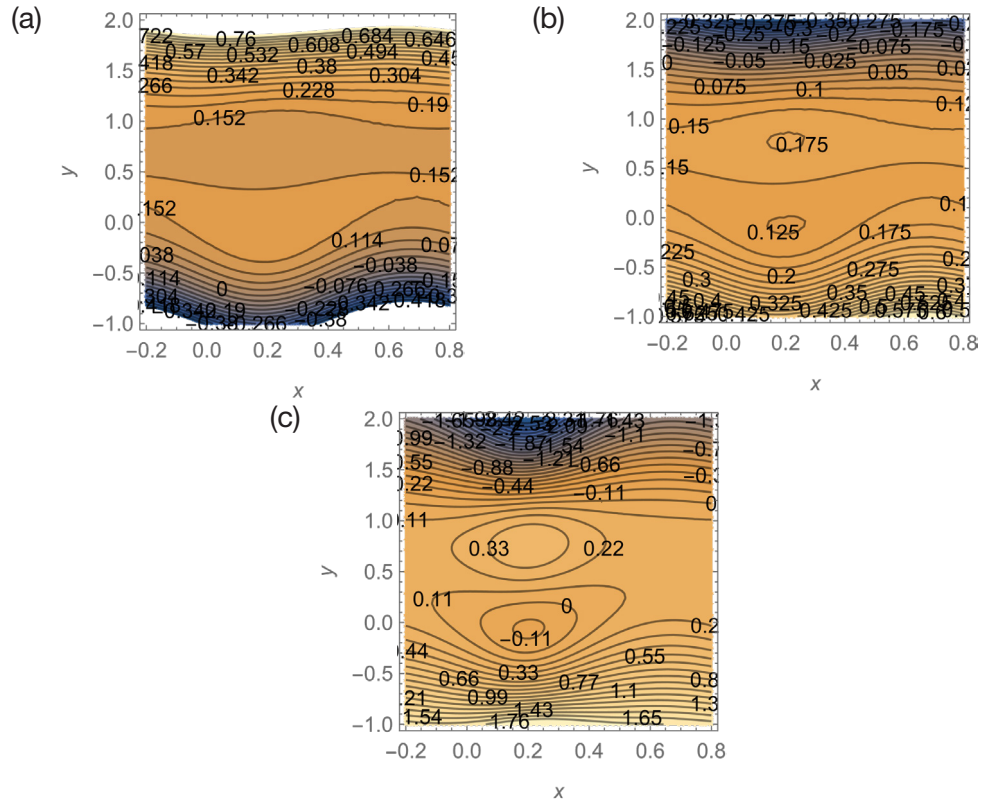

Figure 34: Stream function in the wave frame of (Ω) such that in (a) Ω = 1, (b) Ω = 2, (c) Ω = 3, in Ha = 0.4, Da = 6, $\mu = 0.6$, $\rho = 0.4$, Ø = 0.4, $a = 0.1$, $b = 0.3$, $E_1 = 0.5$, $E = 0.1$, $\beta^* = 0.1$, Rn = 0.3, $\beta_1 = 0.2$.

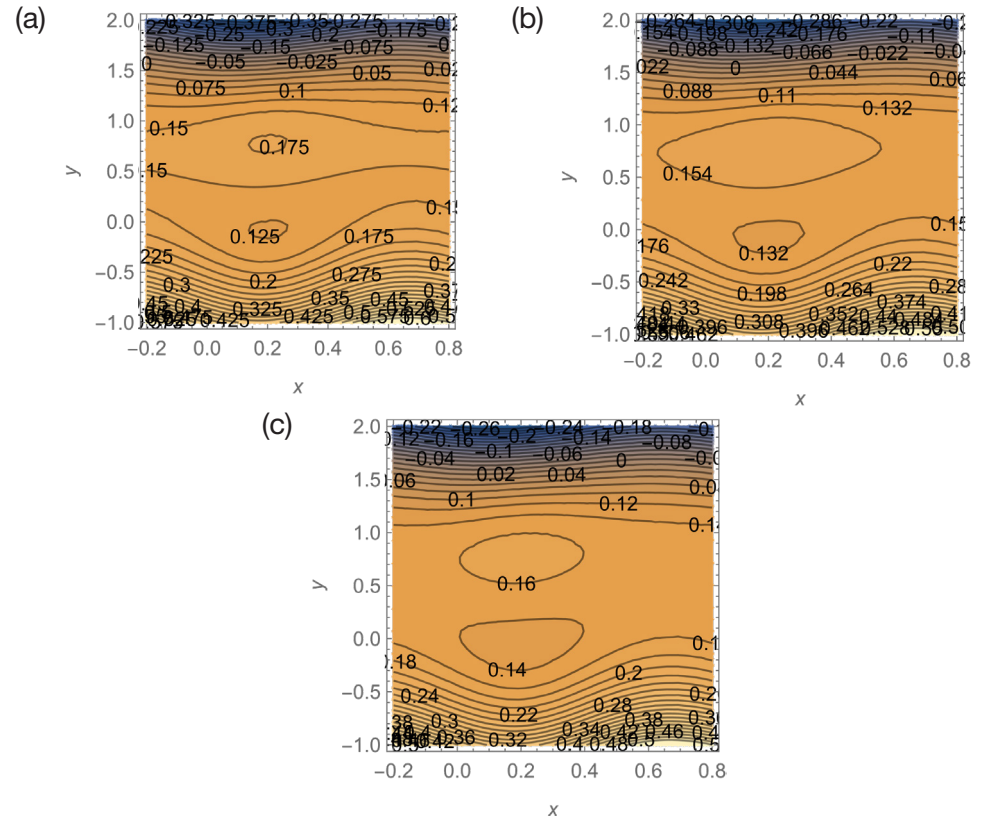

Figure 35: Stream function in the wave frame of (Rn) such that in (a) Rn = 0.3, (b) Rn = 0.4, (c) Rn = 0.5, in Ω = 2, Da = 6, $\mu = 0.6$, $\rho = 0.4$, Ø = 0.4, $a = 0.1$, $b = 0.3$, $E_1 = 0.5$, $E = 0.1$, $\beta^* = 0.1$, Ha = 0.4, $\beta_1 = 0.2$.

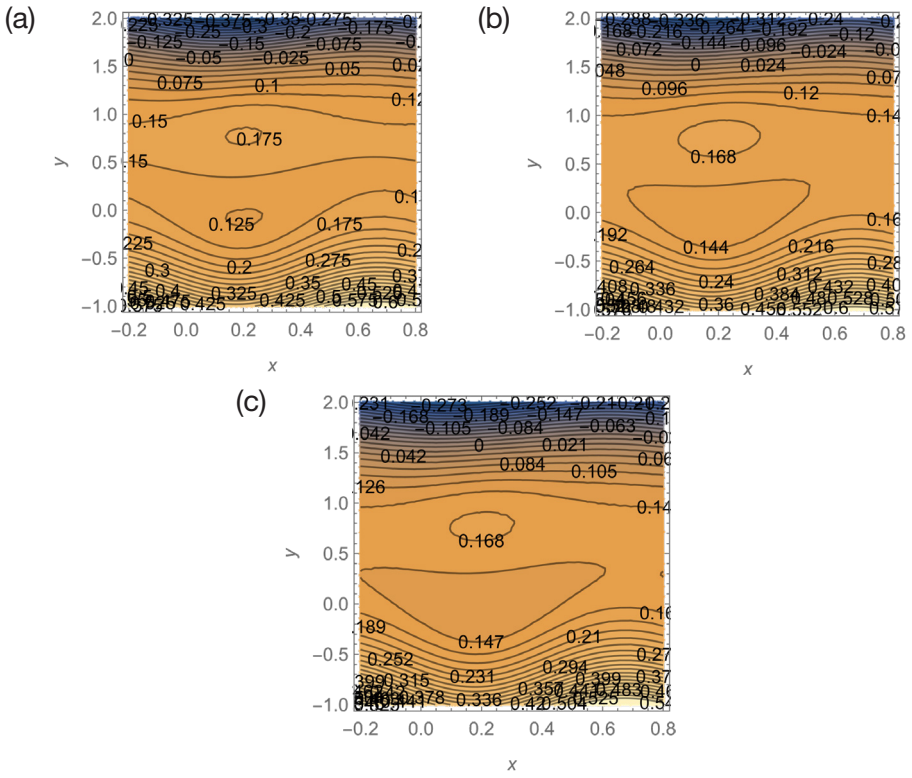

Figure 36: Stream function in the wave frame of (β_1) such that in (a) $\beta_1 = 0.2$, (b) $\beta_1 = 0.4$, (c) $\beta_1 = 0.8$, in $\Omega = 2$, Da = 6, $\mu = 0.6$, $\rho = 0.4$, $\emptyset = 0.4$, $a = 0.1$, $b = 0.3$, $d = 0.5$, $E_1 = 0.1$, $\beta^* = 0.1$, Rn = 0.3, Ha = 0.4.

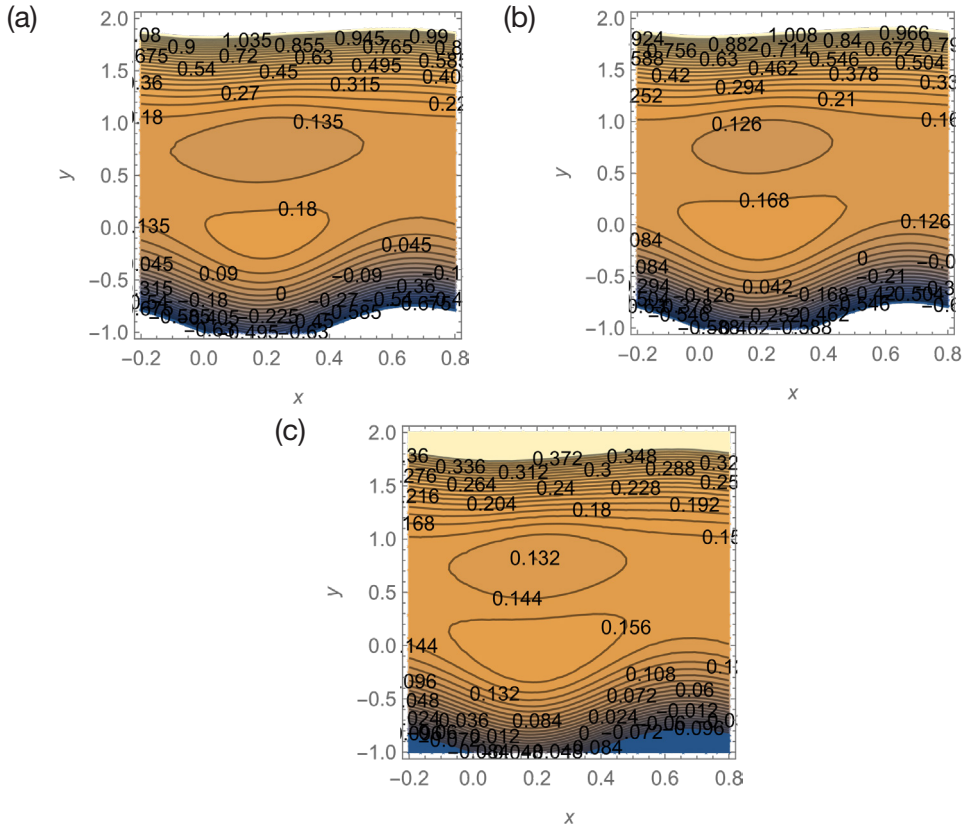

Figure 37: Stream function in the wave frame of (ρ) such that in (a) $\rho = 0.001$, (b) $\rho = 0.02$, (c) $\rho = 0.2$, in $\Omega = 2$, Da = 6, $\mu = 0.6$, Ha = 0.4, $\emptyset = 0.4$, $a = 0.1$, $b = 0.3$, $E_1 = 0.5$, $E = 0.1$, $\beta^* = 0.1$, Rn = 0.3, Ha = 0.4.

References

[1] Srivastava, L. M., and V. P. Srivastava, Peristaltic transport of a non-Newtonian fluid: applications to the vas deferens and small intestine. *Annals of biomedical engineering*, 13, (1985), 137–153.

[2] Hariharan, Prasanna, V. Seshadri, and R. K. Banerjee, Peristaltic transport of non-Newtonian fluid in a diverging tube with different wave forms. *Mathematical and Computer Modelling*, 48 (7–8), (2008), 998–1017.

[3] Narahari, M., and S. Sreenadh, Peristaltic transport of a Bingham fluid in contact with a Newtonian fluid. *Int J Appl Math Mech*, 6 (11), (2010), 41–54.

[4] Frigaard, I.A., Ryan, D. P., Flow of a viscos-plastic fluid in a channel of slowly varying width. *Journal of Non-Newtonian Fluid Mechanics*, 123 (1), (2004), 67–83.

[5] Hayat, Tasawar, M. Umar Qureshi, and Qamar Hussain, Effect of heat transfer on the peristaltic flow of an electrically conducting fluid in a porous space. *Applied Mathematical Modelling*, 33 (4), (2009), 1862–1873.

[6] Srinivas, S., and R. Gayathri, Peristaltic transport of a Newtonian fluid in a vertical asymmetric channel with heat transfer and porous medium. *Applied Mathematics and Computation*, 215 (1), (2009), 185–196

[7] Mekheimer, Kh S., Saleh Zein-Alabedien Husseny, and Y. Abd Elmaboud, Effects of heat transfer and space porosity on peristaltic flow in a vertical asymmetric channel. *Numerical Methods for Partial Differential Equations: An International Journal*, 26 (4), (2010), 747–770

[8] K. S. Mekheimer, Peristaltic flow of a magneto-micropolar fluid: effect of induced magnetic field, *Journal of Applied Mathematics*, (2008), 23. Article ID 570825.

[9] S. K. Pandey and M. K., Chaube, Peristaltic flow of a micropolar fluid through a porous medium in the presence of an external magnetic field, *Communications in Nonlinear Science and Numerical Simulation*, vol. 16, no. 9, pp. 3591–3601, (2011).

[10] Abdulsalam, S.I., Bhatti, M.M., The study of non-Newtonian nanofluid with hall and ion slip effects on peristaltically induced motion in a nonuniform channel. *RSC Advances*, 8 (15), (2018), 7904–7915.

[11] Srinivas, S., R. Gayathri, and M. Kothandapani, The influence of slip conditions, wall properties and heat transfer on MHD peristaltic transport. *Computer Physics Communications*, 180 (11), (2009), 2115–2122.

[12] Lakshminarayana, P., S. Sreenadh, and G. Sucharitha, The influence of slip, wall properties on the peristaltic transport of a conducting Bingham fluid with heat transfer. *Procedia engineering*, 127, (2015), 1087–1094.

[13] Satyanarayana, K. V. V., et al., The effect of wall properties on the convective peristaltic transport of a conducting Bingham fluid through porous medium. *Indian journal of science and technology*, 9 (42), (2016): 1–9.

[14] Sucharitha, G., et al., Peristaltic flow and heat transfer of a Herschel-Bulkley fluid in an inclined non-uniform channel with wall properties. *IOP conference series: materials science and engineering*. Vol. 263. No. 6. IOP Publishing, 2017.

[15] Sucharitha, G., P. Lakshminarayana, and N. Sandeep. Joule heating and wall flexibility effects on the peristaltic flow of magnetohydrodynamic nanofluid. *International Journal of Mechanical Sciences*, 131, (2017), 52–62.

[16] Hayat, T., et al., Peristaltic transport of nanofluid in a compliant wall channel with convective conditions and thermal radiation. *Journal of Molecular Liquids*, 220, (2016), 448–453.

[17] Riaz, Arshad, et al., The influence of wall flexibility on unsteady peristaltic flow of Prandtl fluid in a three-dimensional rectangular duct. *Applied Mathematics and Computation*, 241, (2014), 389–400.

[18] Srinivas, S., and M. Kothandapani, The influence of heat and mass transfer on MHD peristaltic flow through a porous space with compliant walls. *Applied Mathematics and Computation*, 213 (1), (2009), 197–208.

[19] Lakshminarayana, Pallavarapu, et al., Peristaltic slip flow of a Bingham fluid in an inclined porous conduit with Joule heating. *Applied Mathematics and Nonlinear Sciences,* 3 (1), (2018), 41–54.

[20] Kothandapani, M., Srinivas, S., On the influence of wall properties in the MHD peristaltic transport with heat transfer and porous medium. *Physics Letters A*, 372 (25), (2008), 4586–4591.

[21] Srinivas, S., Gayathri, R., Peristaltic transport of a Newtonian fluid in a vertical asymmetric channel with heat transfer and porous medium. *Applied Mathematics and Computation*, 215 (1), 2009, 185–196.

[22] Srinivas, S., Gayathri, R., Kothandapani, M., The influence of slip conditions, wall properties and heat transfer on MHD peristaltic transport. *Computer Physics Communications*, 180 (11), 2009, 2115–2122.

[23] Manjunatha, G., Rajashekhar, C., Vaidya, H., Prasad, K.V., Peristaltic mechanism of Bingham liquid in a convectively heated porous tube in the presence of variable liquid properties. *Special Topics & Reviews in Porous Media: An International Journal*, 10 (2), 2019, 1–10.

[24] Vaidya, H., Rajashekhar, C., Manjunatha, G., Prasad, K.V., Effect of variable liquid properties on peristaltic flow of a Rabinovitch fluid in an inclined convective porous channel. *The European Physical Journal Plus*, 134 (5), 2019, 231.

[25] Divya, B., Manjunatha, G., Rajashekhar, C., Hanumesh, V., Prasad, K., Impact of variable liquid properties on Peristaltic mechanism of convectively heated Jeffrey fluid in a slippery elastic tube. *Frontiers in Heat and Mass Transfer*, 12, 2018, 15.

[26] B.B. Divya, G. Manjunatha, C. Rajashekhar, H. Vaidya, K.V. Prasad, Effects of Inclined Magnetic Field and Porous Medium on Peristaltic Flow of a Bingham Fluid with Heat Transfer Journal of Applied and Computational Mechanics, Vol. 7, No. 4, (2021), 1892–1906.